International Journal of Hydrogen Energy 126 (2025) 368–375

Contents lists available at ScienceDirect

International Journal of Hydrogen Energy

journal homepage: www.elsevier.com/locate/he

Stabilization of premixed flames in narrow channels by a highly conductive embedded wall segment: Application to hydrogen-air mixtures

Carmen Jiménez [a,*], Antoine Pestre [b], Bénédicte Cuenot [b,1], Vadim N. Kurdyumov [a]

[a] Energy Dept., CIEMAT, Avda. Complutense 40, Madrid, 28040, Spain
[b] CERFACS, 42, Av. Gaspard Coriolis, Toulouse, 31100, France

ARTICLE INFO

Keywords:
Hydrogen combustion
Lean hydrogen-air flames
Micro-scale combustion
Heat recirculation
Flame stabilization
Heated channels

ABSTRACT

This study uses numerical analysis to investigate the potential for stabilizing hydrogen-air flames within narrow channels by incorporating a wall segment of finite length with high thermal conductivity. The numerical model is based on the Navier–Stokes equations, coupled with energy and mass conservation equations for reacting gases, and incorporates detailed chemistry and transport models, including thermal diffusion (the Soret effect). For the gas–solid coupling, a novel computational method is used that avoids the expensive calculations associated with solving the unsteady conjugate gas–solid heat transfer.

For the first time, we demonstrate that this innovative thermal stabilization method provides stable operation for lean hydrogen-air combustion across a wide range of reactant flow rates. This offers significant flexibility in terms of power output variation, surpassing the performance of classical counterflow heat recirculating devices. Finally, this study emphasizes the importance of incorporating the Soret effect in the species transport model to accurately compute hydrogen-containing flames, especially in highly curved flame configurations.

1. Introduction

Small-scale combustion has received significant recent interest as a power and heat generation technology for portable electronic or micro-mechanical devices [1,2]. This is because it offers advantages over existing small-scale batteries, such as low weight, small size, high power output, fast recharging, and long duration. Moreover, hydrogen-fueled small-scale combustion systems are carbon neutral, and their NOx emissions can be reduced by operating at lean or ultra-lean conditions [3,4].

Flame stabilization poses a significant challenge in the design of small combustion devices. In these systems, the short residence times and large surface-to-volume ratios result in a large percentage of the heat produced in the combustion process being lost through the walls or carried away from the device with the hot products, leading to flame destabilization or even extinction. The main techniques used to increase flame stability and combustion efficiency in small-scale devices are based on designs that introduce flow recirculation, heat recirculation, or a combination of the two, and are reviewed in [1,2,5].

Heat-recirculating techniques involve harvesting part of the combustion-produced heat and recirculating it to the fresh reactants, either via a solid material (such as the device walls [6] or an immersed porous matrix [7–9]), through heat exchange in counter-flowing parallel channels as in the pioneering works of Lloyd and Weinberg [10–12] or the more recent analyses in [13] or [14], or, alternatively, through exchange in co-flowing parallel channels as in [15]. These techniques have been extensively studied since the 1970s using analytical and numerical methods, with different approximations for the chemical kinetics of combustion.

In the case of parallel counter-flowing channels, in particular, numerical analysis has shown that effective heat exchange is achieved by narrowing the channels, as well as by carefully choosing the thermal properties of the wall material and its thickness (see, for example, the asymptotic analysis of superadiabatic flames in channels in [16,17], complemented by numerical work using Arrhenius [18] and chain-branching [19] kinetics). Generally, numerical models assume thin walls [18,19], so the temperature variation across the walls can be approximated as linear. In this case, the heat exchange rate between the gas and the channel wall can be assumed to be proportional to the temperature difference across the wall, with a factor given by the ratio of the heat conductivities of the wall material and the gas and the inverse of the wall thickness. This has been shown to be a good approximation for sufficiently thin walls in [19], using asymptotic analysis. According

* Corresponding author.
E-mail address: carmen.jimenez@ciemat.es (C. Jiménez).
[1] Present affiliation: Safran Aircraft Engines.

https://doi.org/10.1016/j.ijhydene.2025.03.358
Received 16 December 2024; Received in revised form 22 February 2025; Accepted 26 March 2025
Available online 11 April 2025

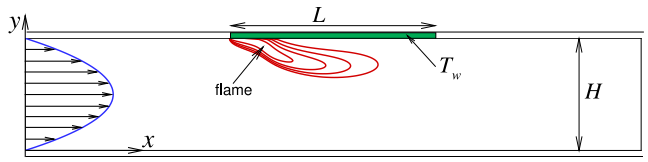

Fig. 1. Sketch of the problem.

to this model, thin walls with low thermal conductivities would reduce heat recirculation, but a very high conductivity of the wall would result in large heat losses and lead to flame extinction.

A recent study [20] examined the case where the flame is stabilized in a channel by interacting with a highly conductive wall segment of finite length, acting as a flame holder. In that study, it was assumed that the thermal conductivity of the segment material was so high that its temperature (unknown in advance) was uniform, which helped decouple the gas and solid problems. Additional simplifications, such as a constant density assumption, constant transport properties, a unity Lewis number for the fuel, and one-step global Arrhenius kinetics, were used. Results showed that with a highly conductive segment of the wall acting as a flame holder, a steady-state flame can be obtained for a large range of inflow velocities of the reactants. For the case of an isolated narrow channel, the flame could be sustained under inflow velocities of the order of 10–20 times the laminar flame speed, much larger than the maximum flow rate obtained in standard heat recirculation devices, where the range of flow rates for stationary solutions is between 2–5 times the laminar flame speed [5]. Nevertheless, because of the mentioned simplifications, these results could not be considered quantitatively accurate.

The purpose of the present work is to explore this novel concept of flame stabilization in the case of lean hydrogen/air combustion in narrow channels, using the full Navier–Stokes equations and detailed chemical kinetics and transport properties (including the Soret effect). This is a case of practical interest because burning hydrogen in lean conditions effectively reduces NOx emissions. The main goals are to extend the results of [20] to a more realistic set-up, taking into account thermal expansion and realistic kinetics and transport models, and also to estimate the range of parametric values that would ensure stable hydrogen flames, confirming that this stabilization method is potentially useful. Since calculations with detailed kinetics for hydrogen-air mixtures require significantly more numerical effort, this work will not present an exhaustive parametric analysis, but will instead focus on demonstrating the feasibility of lean hydrogen flame stabilization. For simplicity, we assume an isolated channel, but the formulation can be easily extended to include heat losses to the environment or systems of parallel co-flowing or counter-flowing channels, as proposed in [20].

2. Mathematical formulation and numerical treatment

Consider a hydrogen/air mixture at initial temperature T_0 flowing at a mean velocity U in a planar channel of width H. The channel walls are assumed to be adiabatic, except for a segment of length L, the flame holder, which is made of a material with high thermal conductivity (asymptotically infinite), embedded in one of the walls, and isolated from the external environment. The sketch in Fig. 1 illustrates this problem.

Previous investigations studying freely propagating flames in a narrow channel have shown that, because of the high diffusivity of hydrogen, the stable solutions for lean hydrogen flames can be non-symmetric with respect to the channel axis [21]. Anticipating this possibility, symmetric wall conditions are avoided, and the conductive segment is placed in one of the channel walls in the present study.

The high conductivity of the flame holder results in a uniform temperature of the wall segment, T_w, which is a priori unknown and needs to be obtained as part of the problem solution. This uniform temperature condition can be obtained by a rigorous mathematical expansion in terms of a small parameter (the ratio of the gas to the solid thermal conductivities) [22], and has been used in previous works to simplify the modeling of heat exchange between a reacting gas and a wall [20,22], a porous plug [23] or a solid body [24].

In the present study, instead of numerically solving the complete problem with conjugate heat transfer between a solid and a reacting gas, we use another methodology already presented in [20]. As a first step, a series of auxiliary problems in which the uniform temperature of the conducting wall segment, T_w, is externally fixed are solved for several T_w values. The total heat flux from the reacting gas to the wall is calculated for each of the obtained steady-state solutions. If the heat flux becomes zero for certain values of the imposed segment temperature T_w, these temperature values correspond to the steady-state solutions of the original problem, where the conductive wall segment is in contact only with the flame and is isolated from the external environment.

It should be noted that we solve two different problems by this method. The first problem is that of a flame in a channel with a highly conductive wall segment in which a given temperature T_w is maintained by external means. This problem is solved by integrating the gas conservation equations with the adequate wall boundary conditions, by which the L size wall segment is isothermal with temperature T_w. Each of these computations is, therefore, relatively straightforward and inexpensive, with the gas equations decoupled from the heat equation in the solid material, which would typically imply large computation times.

The second problem is to find which of the solutions of the first problem results in a net-zero heat flux between the reacting gas and the conductive segment, thus corresponding to a steady-state solution of the conjugate heat transfer problem. This problem is solved by computing the heat flux from the gas to the wall for each of the previous solutions, as presented further below.

According to the authors, this strategy for finding steady-state solutions is simpler and cheaper than solving the conjugate gas–solid heat transfer problem for the following reasons. Firstly, the present method can be implemented in any reacting gas solver with no modifications because the wall segment is represented just as an isothermal boundary condition on the wall. There is no need to establish a conforming mesh for the solid and gas equations. Secondly, for segments with a high thermal capacity, the problem has two very different characteristic times. The first is associated with the gas phase, while the other, much larger, is determined by the high thermal capacity of the segment. This can lead to excessive numerical costs, since the numerical time step would be determined by the fast dynamics and chemical reactions in the gas phase, while the total time required to establish a steady-state solution would be determined by the large characteristic thermal time for the solid segment.

In writing the gas governing equations below, we neglect body forces and radiation effects. Radiation between the gas and the walls can have some effect on the heat transfer [5], but we neglect it in the present work and study only heat conduction effects as a first step. The steady-state conservation equations for mass, momentum, energy and species mass fractions are:

$$\boldsymbol{\nabla}\cdot(\rho\mathbf{v})=0, \tag{1}$$

$$\boldsymbol{\nabla}\cdot(\rho\mathbf{v}\mathbf{v})=-\boldsymbol{\nabla}p+\boldsymbol{\nabla}\cdot\tau, \tag{2}$$

$$\boldsymbol{\nabla}\cdot(\rho e\mathbf{v})=\boldsymbol{\nabla}\cdot(-p\mathbf{v}+\tau\cdot\mathbf{v})-\boldsymbol{\nabla}j_q, \tag{3}$$

$$\boldsymbol{\nabla}\cdot\left(\rho Y_i\mathbf{v}\right)=-\boldsymbol{\nabla}\cdot\mathbf{j}_i+\dot{\omega}_i, \tag{4}$$

where $i=1,\ldots,N$ and ρ, $\mathbf{v}$, $e=e_i+\frac{v^2}{2}$ and Y_i represent, respectively, the density, velocity, energy per unit mass and mass fraction of species i, p is the pressure, τ the viscous stresses tensor, $\mathbf{j}_q$ the heat flux (which

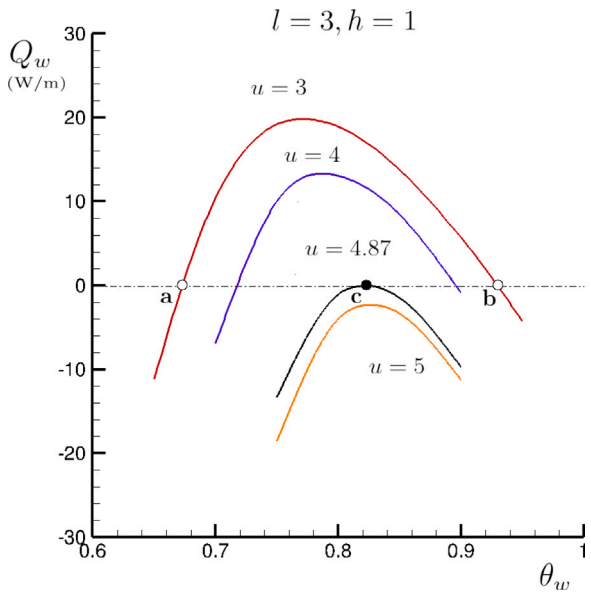

Fig. 2. The net heat flux from the gas to the wall Q_w, as a function of the segment temperature θ_w, for the solutions of the auxiliary problem (fixed θ_w) for $h = 1$ and $l = 3$ at increasing reactant flow rates u. Regions where $Q_w > 0$ correspond to heating of the wall in Eq. (6); regions with $Q_w < 0$ correspond to wall cooling. The values of θ_w for which $Q_w = 0$ select the steady-state solutions of the conjugate problem for each u, which are double solutions in the general case (two wall temperature values for each inlet velocity, as f. ex. **a** and **b** for $u = 3$). The dark circle **c** indicates the critical value $u \approx 4.87$, beyond which there are no solutions of the conjugate problem.

includes the conductive flux and the diffusive transport of partial enthalpies), $\mathbf{j}_i$ represents the diffusion flux of species i, and $\dot{\omega}_i$ the mass of species i produced by chemical reactions per unit volume and time.

To solve this problem, we solve a two-dimensional version of Eqs. (1)–(4) in a rectangular domain using the unsteady compressible solver NTMIX, a parallel solver designed for the direct numerical simulation of flames with detailed chemistry, thermodynamics and transport [25]. This solver has been in use for years and validated in numerous previous works, such as in DNS of turbulent hydrogen flames [25], in laminar hydrogen flame-wall interaction simulations [26], in studies of turbulent stratified propane flames [27] or, more recently, in studies of acoustic effects in hydrogen and methane flames in [28] or [29]. NTMIX features sixth and eighth-order central differencing schemes and third-order Runge–Kutta time integration. Here, we use a fictitious time step to reach the steady state solution corresponding to Eqs. (1)–(4).

The equation of state for perfect gases, the Navier–Poisson law for the stress tensor, and Fourier's law for the conductive heat flux are used to close the above equations, incorporating a mixture-averaged model for the viscosity and thermal conductivity. Diffusion fluxes are modeled as proportional to molar fraction gradients (Hirschfelder–Curtiss model [30]) with a mixture-averaged diffusivity for each species, estimated from the temperature-dependent binary diffusivities. Note that a correction velocity needs to be incorporated to ensure mass conservation [25]. Species diffusion by temperature gradients, the Soret effect, is included in the present computations following [31,32], where its influence on the onset of cellular instabilities in planar flames, and the shape and heat release rate of curved hydrogen flames, was shown. The detailed San Diego chemical kinetics mechanism [33,34], which models hydrogen-air combustion using 20 elementary reactions between 8 chemically reactive species, and which has been extensively validated, is used to incorporate the reaction rates in Eq. (4). We have chosen to focus on lean hydrogen-air flames, with equivalence ratio $\phi_0 = 0.4$.

Boundary conditions at the inlet boundary are imposed as a Poiseuille velocity profile with mean velocity U driving a mixture of hydrogen-air at temperature $T_0 = 300$ K, initial pressure $p_0 = 1$ atm, and equivalence ratio $\phi = \phi_0$. At the outlet, partially non-reflecting boundary conditions are imposed using the NSCBC methodology [35, 36]. These conditions allow specifying a pressure level at the far field and, at the same time, permit physical or numerical waves to leave the domain. The walls are taken as impermeable, no-slip, and adiabatic, except for the conducting flame holder, located at the upper channel wall, which is taken as isothermal with a temperature T_w, as explained above.

The simulations are initialized using a planar flame solution corresponding to a hydrogen-air flame at $\phi = \phi_0$, located upstream of the flame holder Then, a series of temperature values T_w, ranging from above the adiabatic flame temperature to near the fresh gases temperature, are imposed at the conducting segment. It should be noted that for too low or too high gas flow rates, the flame can propagate upstream (flashback) or downstream (blow-off). This circumstance can occur due to adiabatic conditions on the walls of the channel outside the highly conductive segment. Anticipating the results of numerical calculations, it can be indicated that blow-off is extremely difficult for hydrogen-air mixtures.

During the simulation, the total heat transfer from the gas to the flame holder, Q_w, is computed as:

$$Q_w = \int_0^L q_w(x)dx = -\int_0^L \left(\lambda \frac{\partial T}{\partial y}\right)\Big|_{y=H} dx. \tag{5}$$

A positive value of the heat transfer ($Q_w > 0$) indicates a net heat flux from the reacting gas to the wall segment, while $Q_w < 0$ corresponds to a net flux from the segment to the gas.

In the conjugate problem (not resolved in the present study), the value of the uniform wall segment temperature would be determined by the evolution equation:

$$C\frac{dT_w}{dt} = Q_w. \tag{6}$$

According to Eq. (6), T_w increases for $Q_w > 0$ and decreases for $Q_w < 0$. Here C represents the total thermal capacity of the flame holder, which, in realistic cases of metallic materials, for example, should be much larger than one. In any case, the steady-state solution of the conjugate heat transfer problem between the flame and the isolated wall is independent of the value C and corresponds to the case $Q_w = 0$. Therefore, finding among the solutions of the decoupled (auxiliary) gas problem those that correspond to $Q_w = 0$ determines the steady-state solutions of the conjugate gas–solid system.

To present the results of this investigation and compare them to previous work, it is convenient to use dimensionless parameters and variables. We use the flame propagation speed of the planar unstretched hydrogen-air flame at $\phi = \phi_0$, S_L, and its thermal thickness, $\delta_T = D_T/S_L$, where D_T is the thermal diffusivity of the fresh gas mixture, as scales for velocity and length. The dimensionless channel width and flame holder length are then $h = H/\delta_T$ and $l = L/\delta_T$, and the dimensionless reactants flow rate is $u = U/S_L$. The dimensionless temperatures for the gas and the conductive segment are $\theta = (T - T_0)/(T_a - T_0)$ and $\theta_w = (T_w - T_0)/(T_a - T_0)$, where T is the gas temperature, T_0 its value in the fresh gases stream, and T_a is the adiabatic temperature of the planar flame. Here, the values for these scales correspond to a hydrogen-air flame at equivalence ratio $\phi_0 = 0.4$ and standard pressure and temperature conditions, and are reported in Table 1.

The calculations are carried out in a rectangular domain with $x/\delta_T = [-5 : l + 10]$ and $y/\delta_T = [0, h]$, discretized on a uniform square grid with $\Delta x/\delta_T = 1/30$. The conducting wall segment is located at $x = 0$. The grid size, with 30 points inside the thermal flame thickness, guarantees sufficient resolution for the reaction zone. Grid refinement studies have been conducted, showing that the computed Q_w at a resolution $\Delta x/\delta_T = 1/40$ changes by only 2%. We also verified that increasing the domain length did not affect the results.

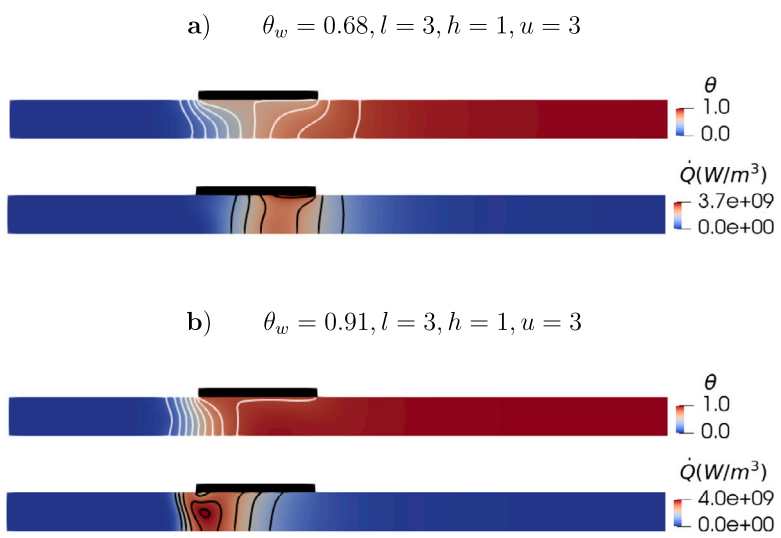

Fig. 3. The temperature (θ) and heat release rate ($\dot{Q}$) fields for the double steady state flame solutions marked as **a** and **b** in Fig. 2, corresponding to $h = 1$, $l = 3$ and $u = 3$. The thin white lines are isocontours at $\theta = 0.1, 0.2, \ldots, 0.9$ and the black lines are isocontours at $\dot{Q}/\dot{Q}_{max} = 0.3, 0.5, 0.7, 0.9$ and 0.99.

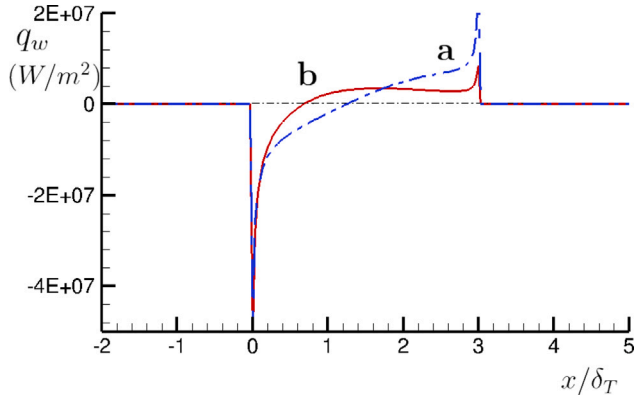

Fig. 4. Local heat flux profiles along the gas-wall boundary for the solutions marked as **a** and **b** in Fig. 2 and represented in Fig. 3, corresponding to a segment of length $l = 3$.

Table 1
Simulation and scaling parameters.

ϕ_0	S_L (cm/s)	δ_T (mm)	T_a (K)	$h = H/\delta_T$	$l = L/\delta_T$
0.4	22.8	0.15	1423	1	3, 5

3. Results

Despite the simplifications in the formulation of the problem, the total number of parameters is quite large, making a complete parametric analysis difficult. For this reason, the study is carried out only for a selected set of parameters. All the results presented below correspond to a flame at $\phi_0 = 0.4$, $T_0 = 300$ K and $p = 1$ atm, in a channel of width $h = 1$, and to a wall segment made of a material of very high conductivity (asymptotically infinite) and with dimensionless length $l = 3$ and $l = 5$, as reported in Table 1. The dimensionless flame holder temperature is varied from $\theta_w \approx 1.3$ to $\theta_w \approx 0$.

Due to the simplifying assumption of adiabatic walls outside the stabilizing element, for sufficiently small reactant flow rates, u, the flame can propagate upstream. This is known as the flashback effect, and in this case the flame holder is of no use in stabilizing the flame. For sufficiently large reactant flow rates, the flame is blown off outside of the channel. The determination of the critical values of the flashback and blowoff conditions remains outside the scope of this work. In classical counterflowing heat recirculation devices, the flame can be stabilized typically for an inflow rate range between $u = 2$ and $u = 5$ approximately [5]. As will be shown below, with the present stabilization technique, the range of inflow rates can be extended if the conducting wall segment is sufficiently long. For each flame holder, the imposed reactant flow is therefore varied from a value $u > 1$ to the critical value above which the flame can no longer be stabilized and is blown off.

Fig. 2 presents results for a flame in a channel with a conducting segment of length $l = 3$. The curves correspond to the computed net heat flux at different imposed segment temperatures, $Q_w(\theta_w)$, for increasing values of the reactant flow rate u. It is shown that for moderate values of the flow rate (e.g. $u = 3$ or $u = 4$), the curves cross the $Q_w = 0$ axis at two points. These are the two steady-state solutions of the coupled problem, one corresponding to a hot wall and the other to a colder wall. For $u = 3$, the cold and hot wall solutions correspond to the points marked as **a** and **b**, respectively, in Fig. 2. For $u \approx 4.87$ the conjugate problem has only one steady-state solution, at $\theta_w \approx 0.825$, marked as **c** in Fig. 2. This corresponds to the critical reactant flow rate value for this wall segment length, above which there are no steady-state solutions of the conjugate problem. For faster flow ($u > 4.87$) the flame cannot be stabilized at the conducting wall segment and is blown off.

The two steady-state solutions marked as **a** and **b** in Fig. 2, are illustrated in Fig. 3, where the temperature and heat release rate fields of the two flames are plotted. The local heat flux from the gas to the solid, computed along the gas/wall boundary as $q_w = -\left(\lambda \frac{\partial T}{\partial y}\right)\Big|_{y=H}$, is plotted in Fig. 4 for the two solutions corresponding to $Q_w = 0$. It is evident that the two simultaneous flame solutions appearing for the same set of parameters (e.g., $h = 1, l = 3, u = 3$) are very different in shape and location, resulting also in different profiles for the heat flux. For case **a**, shown in the top plot of Fig. 3, the flame is located near the middle of the conducting segment, which is then relatively cold, $\theta_w \approx 0.68$. The heat flux for this case, plotted in Fig. 4 with a dashed–dotted line, shows that burnt gases heat the downstream half segment ($q_w > 0$), with the magnitude of the transferred heat gradually growing towards a peak at the rear end. The wall preheats fresh gases at the upstream half ($q_w < 0$), with a large negative peak at the upstream end. The flame corresponding to the highest flame holder temperature, $\theta_w \approx 0.91$ (solution **b** at the bottom plot of Fig. 3), is located at the upstream end of the flame holder. In this case, the contact surface between the burnt gases and the conducting wall

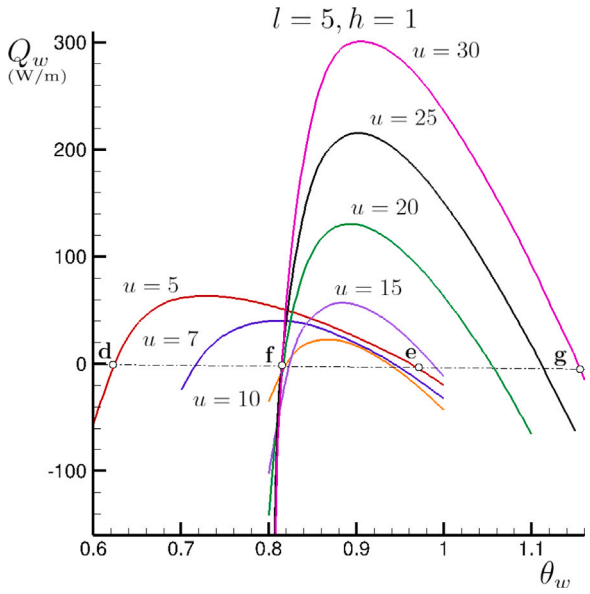

Fig. 5. The net heat flux from the gas to the wall (Q_w) as a function of the segment temperature θ_w for the solutions of the auxiliary problem (fixed θ_w) for $h = 1$ and $l = 5$ at increasing reactant flow rates u. Regions where $Q_w > 0$ correspond to heating of the wall in Eq. (6); regions with $Q_w < 0$ correspond to wall cooling. The values of θ_w for which $Q_w = 0$ select the steady-state solutions of the conjugate problem for each u, as for example the double solutions marked as **d**, **e** and **f**, **g**, for $u = 5$ and $u = 30$, respectively.

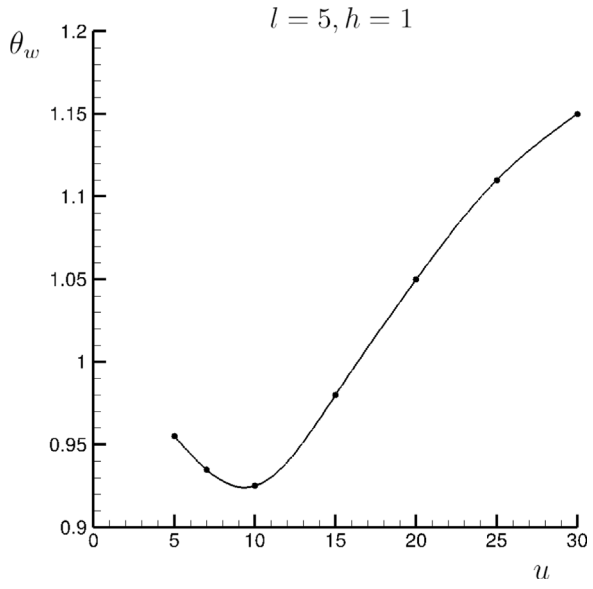

Fig. 6. The wall segment temperature θ_w corresponding to the high temperature (stable) solution for a hydrogen flame in a channel of width $h = 1$ with a flame holder with $l = 5$ as the inflow rate u increases.

segment is larger and the segment temperature is close to the adiabatic flame temperature. The heat flux from the hot gases to the segment is more evenly distributed along the segment length, as seen in Fig. 4 (solid line), while the transfer from the wall to the fresh gases occurs again as a peak at the upstream tip. Anticipating the discussion of the stability of solutions, we should mention that solution **a** is unstable, while solution **b** is stable.

As the flame holder length is increased, the range of values of u for which steady-state flame solutions are found also increases, as shown in Fig. 5 for $l = 5$. Interestingly, for this segment length no critical blow-off rate was detected. Even at very large values of the reactants' flow rate, the flame is still stabilized by its interaction with the conductive segment. At least this is the case for flow rates as large as $u = 30$, as can be seen in the figure. Notice that cases at larger velocities were not computed, as the model assumptions might not be valid beyond $u = 30$.

Two steady-state solutions (with $Q_w = 0$) at two different values of θ_w are also detected in Fig. 5 for each of the values of the flow rate u. The value of the highest wall segment temperature for each flow rate u is shown in Fig. 6 as a function of u. Figs. 7 and 8 illustrate the temperature and the heat release distributions in the channel for the points marked as **d**, **e**, **f** and **g** in Fig. 5.

For moderate flow rates (up to $u \approx 15$, see Fig. 6), the wall temperature values corresponding to the two steady-state solutions are below the adiabatic flame temperature. As u increases up to $u \approx 10$, the net heat flux Q_w decreases, and the values of θ_w for the two steady solutions approach each other. The flame structures are very similar to those found for the shorter segment $l = 3$. This can be appreciated in Fig. 7, for the case with $l = 5, u = 5$. Here, as in the case of $l = 3$, the two steady-state solutions are nearly planar; one is located near the downstream end of the segment, resulting in a rather cold segment temperature (flame **d** at $\theta_w = 0.625$), and the other is located near the upstream end of the segment, leading to a higher wall temperature (flame **e** at $\theta_w = 0.955$). The slightly curved flame in Fig. 7**e** presents already a zone near the bottom wall where the temperature exceeds the adiabatic temperature ($\theta_w > 1$), marked with a thicker white contour.

As u is increased further, the behavior of the response curves changes from what was observed for the shorter segment. Instead of approaching and merging into a single solution at a critical blow-off flow rate, as seen before for $u \approx 4.87$ in Fig. 3, the two steady solutions separate as the value of the higher temperature θ_w shifts towards superadiabatic values, as shown in Fig. 6. These results, showing steady-state flames even at very large flow rates and equilibrium wall temperatures increasing with u, are probably linked to the large diffusivity of hydrogen, which can produce highly curved, intensely burning flames. This behavior was not observed in [20], where only flames with $Le = 1$ were investigated.

The flame structures for the double solutions for $l = 5$ and $u = 30$ are presented in Fig. 8. Compared to what was observed for $u = 5$ in Fig. 7, for $u = 30$ the two values for the flame holder temperature θ_w corresponding to the double steady-state solutions are further apart (at $\theta_w = 0.815$ and 1.15, marked as **f** and **g** in Fig. 5), and the flame shapes change drastically. The flame corresponding to the hottest wall (solution **g**) is a long, highly curved flame anchored near the upstream end of the flame holder and extending far behind it. The coldest wall solution (solution **f**) also presents large curvature, but it is located further downstream. For both solutions, the gas temperature largely exceeds the adiabatic flame temperature, reaching values above $\theta = 1.2$, as corresponds to highly stretched hydrogen flames. For the flame anchored upstream (**g**), the contact surface between the hot gases and the conducting wall segment is large, and therefore, the flame holder temperature is very high ($\theta_w = 1.15$). For flame **f**, only moderate-temperature gases are in contact with the conducting wall, the superadiabatic gases are far downstream, and for this reason, the conducting wall segment remains at a moderate temperature ($\theta_w = 0.815$).

The following considerations can be made regarding the stability of the solutions for the conjugate problem for cases with $Q_w = 0$. These considerations are qualitative and, as shown in [20], must be verified by numerical analysis (which was not carried out in the present study). Although all the calculations above were carried out for a fixed temperature of the conductive segment, the response curves' shapes allow us to draw conclusions about the stability of the steady states corresponding to $Q_w = 0$. Indeed, with high probability, the state corresponding to the hottest temperature of the segment is stable, since, according to Eq. (6), with a small increase in T_w at the point

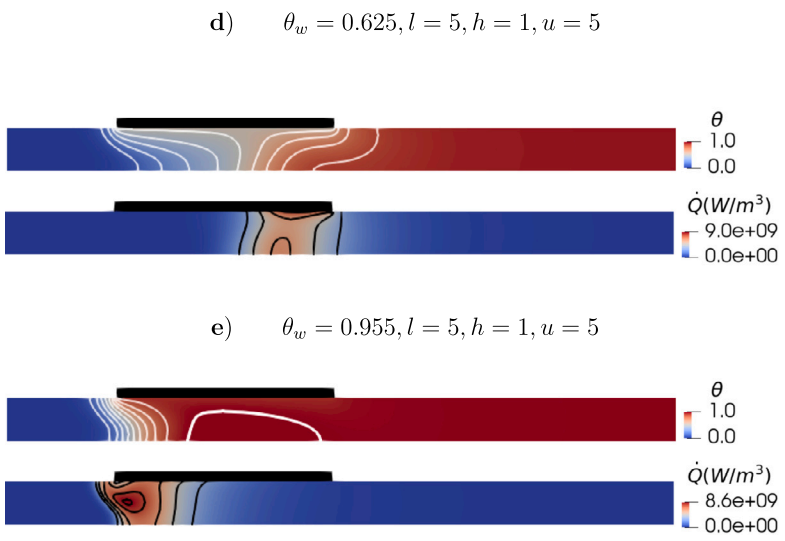

Fig. 7. The temperature (θ) and heat release rate ($\dot{Q}$) fields for the double steady state solutions marked **d** and **e** in Fig. 5, corresponding to $h = 1$, $l = 5$ and $u = 5$. The thin white lines are isocontours at $\theta = 0.1, 0.2, \ldots, 0.9$; thicker white lines are isocontours at and above the adiabatic temperature, $\theta = 1, 1.1, 1.2$; and the black lines correspond to $\dot{Q}/\dot{Q}_{max} = 0.3, 0.5, 0.7, 0.9$ and 0.99. These plots do not include the whole computational domain.

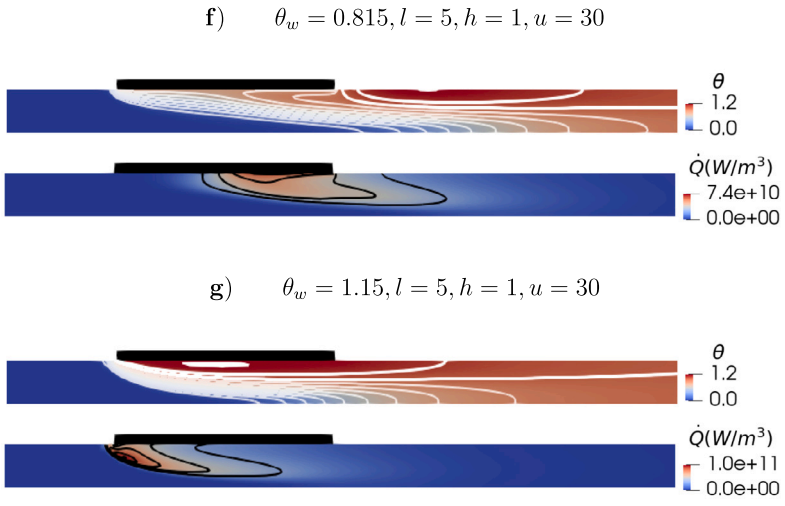

Fig. 8. The temperature (θ) and heat release rate ($\dot{Q}$) fields for the double steady-state solutions marked as **f** and **g** in Fig. 5, corresponding to $h = 1$, $l = 5$ and $u = 30$. The thin white lines are isocontours at $\theta = 0.1, 0.2, \ldots, 0.9$; thicker white lines are isocontours at and above the adiabatic temperature, $\theta = 1, 1.1, 1.2$; and the black lines correspond to $\dot{Q}/\dot{Q}_{max} = 0.3, 0.5, 0.7, 0.9$ and 0.99. These plots do not include the whole computational domain.

corresponding to $Q_w = 0$, the heat flux to the segment becomes negative and the segment must cool down. If the temperature of the segment decreases slightly, the opposite occurs, and the segment temperature increases. For the state with the lower T_w, the response curve has a positive slope at the point corresponding to $Q_w = 0$, which, according to the same reasoning, indicates the instability of this state. Of course, these considerations cannot replace a rigorous stability analysis or time-dependent calculations, which will be given elsewhere. It is also worth noting that when studying the stability of a steady-state solution ($Q_w = 0$) of the conjugate problem, the value of the parameter C appearing in Eq. (6) will play a role.

It is also interesting to pay attention to the following circumstances. A comparison of the response curves in Fig. 5 shows that the maximum of the curve with $u = 10$ is located lower than for the case of $u = 5$. However, this maximum value increases for higher values of u, starting with the curve with $u = 15$. In this case, the θ_w value for the hottest mode corresponding to $Q_w = 0$ also increases with increasing values of u, as represented in Fig. 6. All this means that with a gradual increase in u, the hottest mode with $Q_w = 0$ does not disappear, but, on the contrary, stabilizes. It is reasonable to associate this behavior with the high diffusivity (small Lewis number) of the fuel. Indeed, as the flow rate increases, the curvature of the flame at the wall increases due to an increase in the velocity gradient near the wall, which in turn leads to an increase in the flame temperature. Note that this effect is due only to the high diffusivity of hydrogen because it was not observed in [20] for cases where $Le = 1$. This phenomenon will be discussed in detail elsewhere.

For all the results presented above, thermal diffusion (the Soret effect) was included in the model. To assess the relevance of the Soret effect in the present configuration, we compare in Fig. 9 curves from Fig. 5 to those obtained without the inclusion of the Soret effect, for $l = 5$ and two values of the inflow rate, $u = 5$ and $u = 30$. It is evident that, while for $u = 5$ the effects of thermal diffusion are very small, they become important in the case of large inflow rates, when the flame curvature is large, as seen in Fig. 9 for $u = 30$. Neglecting the Soret effect for this inflow rate would predict a smaller net heat flux and

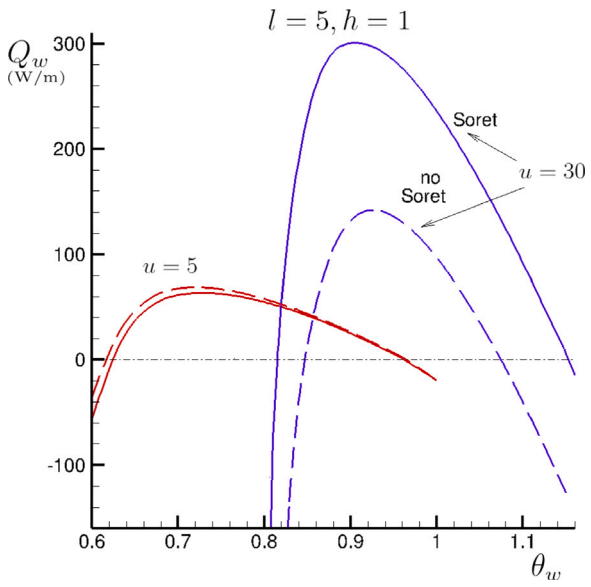

Fig. 9. The net heat flux to the wall (Q_w) as a function of the segment temperature (θ_w) for $h = 1$, $l = 5$ and two values of the inflow rate ($u = 5$ and $u = 30$), computed with and without the Soret effect.

steady-state solutions located at closer values of θ_w; in particular, the wall segment temperature would remain below the adiabatic value for these parameters.

4. Conclusions

The main goal of this work is to demonstrate the possibility of stabilizing a hydrogen-air flame by the effect of a highly conductive wall segment acting as a flame holder. The present results show that for a lean hydrogen-air flame in a channel of height comparable to the thermal flame thickness, a segment of length below 1 mm is enough to obtain steady-state flames for reactant flow rates of the order of 30 times the laminar flame speed, exceeding the performance of classical heat recirculating techniques. This better performance and flexibility in terms of power output allows for more compact systems compared to devices based on heat recirculation through co-flowing or counter-flowing parallel channels. Moreover, these innovative systems are also more flexible in terms of fuel composition, and manufacturing becomes easier, since no miniature bodies inside the channel or moving components are needed.

The calculation method is based on the assumption of high thermal conductivity and, therefore, uniform temperature of the segment. Then, the auxiliary problem of flame stabilization by a highly conductive wall segment with a fixed temperature is solved first, for a series of values of the segment temperature θ_w. If the total heat flux between the segment and the reacting gas, Q_w, becomes zero for certain values of the imposed temperature, these solutions correspond to steady-state solutions of the conjugate heat transfer problem. It is important to note that the conductive wall segment is in contact only with the flame and is isolated from the external environment.

It is shown that double solutions corresponding to the condition $Q_w = 0$ may be obtained. For moderate flow rates, the resulting flames are nearly planar. One is located upstream and corresponds to a hot wall segment, near the adiabatic flame temperature, while the other is located further downstream and corresponds to a relatively cold wall segment. For higher flow rates, the flames present appreciable curvatures and superadiabatic temperatures, as corresponds to curved lean hydrogen flames. The two solutions in this case result in hot wall segments, with temperatures above the adiabatic flame temperature for the solution in which the flame is located upstream. It can be pointed out that, of the two solutions found with $Q_w = 0$, only one, the one with the highest wall temperature value, is stable when the temperature of the segment is not fixed.

Finally, we show that excluding thermal diffusion (the Soret effect) may result in large differences in the obtained solutions. This highlights the importance of including the Soret effect in the species transport model to obtain good predictions for hydrogen flames.

As a continuation of this work, we will investigate the possibility of burning ultra-lean hydrogen mixtures (below the flammability limit) in these devices. Another future avenue of research will explore the potential existence of multiple stable solutions in such devices, as reported in [20] for wider channels, as this could pose safety concerns.

CRediT authorship contribution statement

Carmen Jiménez: Writing – review & editing, Writing – original draft, Visualization, Validation, Software, Resources, Project administration, Methodology, Investigation, Funding acquisition, Formal analysis, Data curation, Conceptualization. **Antoine Pestre:** Writing – review & editing, Visualization, Validation, Software, Resources, Methodology, Investigation, Conceptualization. **Bénédicte Cuenot:** Writing – review & editing, Writing – original draft, Visualization, Validation, Supervision, Software, Resources, Project administration, Methodology, Investigation, Formal analysis, Conceptualization. **Vadim N. Kurdyumov:** Writing – review & editing, Writing – original draft, Visualization, Supervision, Resources, Methodology, Investigation, Funding acquisition, Formal analysis, Data curation, Conceptualization.

Declaration of competing interest

The authors declare that they have no known competing financial interests or personal relationships that could have appeared to influence the work reported in this paper.

Acknowledgments

This study was supported by project Green H2-CM from Comunidad de Madrid, Spain, MCIN and NextGenerationEU (PRTR-C17.I1) and #PID2022-139082NB-C52, MICIN/AEI/10.13039/501100011033 and FEDER.

References

[1] Fernández-Pello AC. Micropower generation using combustion: issues and approaches. Proc Combust Inst 2002;29:883–99.
[2] Ju Y, Maruta K. Microscale combustion: Technology development and fundamental research. Prog Energ Combust Sci 2011;37:669–715.
[3] Mondal MNA, Karimi N, Jackson SD, Paul MC. Numerical investigation of premixed hydrogen/air combustion at lean to ultra-lean conditions and catalytic approach to enhance stability. Int J Hydrog Energy 2023;48(47):18100–15.
[4] Du H, Chai WS, Wei H, Zhou L. Status and challenges for realizing low emission with hydrogen ultra-lean combustion. Int J Hydrog Energy 2024;57:1419–36.
[5] Ellzey J, Belmont E, Smith C. Heat recirculating reactors: Fundamental research and applications. Prog Energ Combust Sci 2019;72:32–58.
[6] Bioche K, Vervisch L, Ribert G. Premixed flame-wall interaction in a narrow channel: impact of wall thermal conductivity and heat losses. J Fluid Mech 2018;856:5–35.
[7] Takeno T, Sato K. An excess enthalpy flame theory. Combust Sci Technol 1979;20:73–84.
[8] Masset P, Dounia O, Selle L. Fully explicit formulae for flame speed in infinite and finite porous media. Combust Theor Model 2021;25:785–812.
[9] Kurdyumov V, Fernández-Galisteo D, Jiménez C. Asymptotic study of premixed flames in inert porous media layers of finite width: parametric analysis of heat recirculation phenomena. Combust Flame 2022;241:112109.
[10] Lloyd S, Weinberg F. A burner for mixtures of very low heat content. Nature 1974;251:47–9.
[11] Lloyd S, Weinberg F. Limits to energy release and utilisation from chemical fuels. Nature 1977;257:367–70.
[12] Jones A, Lloyd S, Weinberg F. Combustion in heat exchangers. Proc R. Soc A Math Phys Eng 1978;360:97–115.

[13] Ju Y, Choi C. An analysis of sub-limit flame dynamics using opposite propagating flames in mesoscale channels. Combust Flame 2003;133:483–93.
[14] Fursenko R, Minaev S. Flame stability in a system with counterflow heat exchange. Combust Explos Shock Waves 2005;41:133–9.
[15] Schoegl I, Ellzey J. Superadiabatic combustion in conducting tubes and heat exchangers of finite length. Combust Flame 2007;151:142–59.
[16] Bosch J, Fernández-Galisteo D, Jiménez C, Kurdyumov V. Analytical study of superadiabatic small-scale combustors with a two-step chain-branching chemistry model: lean burning below the flammability limit. Combust Flame 2022;235:1117311.
[17] Bosch J, Fernández-Galisteo D, Jiménez C, Kurdyumov V. Superadiabatic small-scale combustors: asymptotic analysis of a two-step chain-branching combustion model. Proc Combust Inst 2023;39:1927–35.
[18] Kurdyumov V, Fernández-Galisteo D, Jiménez C. Superadiabatic small-scale combustor with counter-flow heat exchange: Flame structure and limits to narrow-channel approximation. Combust Flame 2020;222:233–41.
[19] Bosch J, Fernández-Galisteo D, Jiménez C, Kurdyumov V. Small-scale superadiabatic combustors with a two-step chain-branching chemistry model: asymptotic models and the effect of two dimensionality on lean mixtures burning. Combust Flame 2024;259:113127.
[20] Kurdyumov V, Jiménez C. Flame stabilization in narrow channels by a highly conductive wall segment: application to small-scale combustion devices. Combust Flame 2022;245:112348.
[21] Jiménez C, Fernández-Galisteo D, Kurdyumov V. DNS study of the propagation and flashback conditions of lean hydrogen-air flames in narrow channels: Symmetric and non-symmetric solutions. Int J Hydrog Energy 2015;40:12541–9.
[22] Kurdyumov V, Jiménez C. Flame stabilisation by a highly conductive body: multiple steady-state solutions and time dependent dynamics. Combust Theor Model 2022;26:669–85.
[23] Matalon M, Kurdyumov V. The porous plug burner: flame stabilization. Onset Oscil Restabilization, Combust Flame 2008;153:105–18.
[24] Dejoan A, Jiménez C, Kurdyumov V. Flame stabilisation by a highly conductive cylinder: Multiple steady-state solutions and dynamics. Proc Combust Inst 2024;40:105205.
[25] Baum M, Poinsot T, Haworth D, Darabiha N. Direct numerical simulation of $h_2/o_2/n_2$ flames with complex chemistry in two–dimensional turbulent flows. J Fluid Mech 1994;281:1–32.
[26] Popp P, Smooke M, Baum M. Heterogeneous/homogeneous reaction and transport coupling during flame–wall interaction. Proc Combust Inst 1996;26:2693–700.
[27] Jiménez C, Cuenot B, Poinsot T, Haworth D. Numerical simulation and modeling for lean stratified propane-air flam. Combust Flame 2002;159:1–21.
[28] Jiménez C, Quinard J, Graña-Otero J, Schmidt H, Searby G. Unsteady response of hydrogen and methane flames to pressure waves. Combust Flame 2022;159:1894–908.
[29] Brouzet D, Talei M, Brear M, Cuenot B. The impact of chemical modelling on turbulent premixed flame acoustics. J Fluid Mech 2021;915:3.
[30] Hirschfelder JO, Curtiss CF, Bird RB. Molecular theory of gases and liquids. New York: Wiley; 1954.
[31] García-Ybarra P, Clavin P. Cross-transport effects in non-adiabatic premixed flames. Prog Astronaut Aeronaut 1981;76:463–81.
[32] Grcar J. A new type of steady and stable, laminar, premixed flame in ultra-lean, hydrogen-air combustion. Proc Combust Inst 2009;32:1011–8.
[33] Saxena P, Williams F. Testing a small detailed chemical–kinetic mechanism for the combustion of hydrogen and carbon monoxide. Combust Flame 2006;145:316–23.
[34] Sánchez AL, Williams FA. Recent advances in understanding of flammability characteristics of hydrogen. Prog Energy Combust Sci 2014;41:1–55.
[35] Poinsot T, Lele S. Boundary conditions for direct simulations of compressible reacting flows. J Comput Phys 1992;101:104–29.
[36] Baum M, Poinsot T, Thévenin D. Accurate boundary conditions for multicomponent reactive flows. J Comput Phys 1995;116:247–61.